5

The bounded layer model

The term "bounded model" in our discussion pertains to a configuration analogous to the classical Rayleigh–Bénard thermal convection problem. A fluid layer is located between rigid and slippery (i.e., stress-free) horizontal surfaces with constant prescribed values of temperature and salinity, as illustrated in Figure 5.1. This model plays an interesting role in the development of double-diffusive theory. The simplicity of its setup has led to the first major breakthroughs in the analysis of finite amplitude effects. The bounded model continues to attract considerable attention from theorists, who use it as a testing ground for the development of analytical techniques and new insights into the mechanics of double-diffusion. At the same time, the application of the model to observable double-diffusive phenomena is far from straightforward. The rigid horizontal planes – an essential component of the bounded model – are absent in most geophysical situations. In the ocean, double-diffusive regions are too separated from the bottom and sea-surface to be influenced by the vertical boundaries. Therefore, each application of the bounded model needs to be carefully and pervasively motivated. We start with the diffusive case (Fig. 5.1a), which is given priority for two reasons. One is historical: the first nonlinear treatment of the bounded model was offered for the diffusive configuration. Another consideration involves a more direct connection of the diffusive bounded model to observable structures.

5.1 Diffusive layer

It is perhaps only natural that the first successful nonlinear treatment of the bounded double-diffusive model was built on, and inspired by, the techniques and insights already developed for thermal convection. Veronis (1965, 1968) examined the role of a stabilizing salt gradient in thermal convection, analyzing linear and leading-order finite amplitude effects. Temperature and salinity values were prescribed at the vertical boundaries of the horizontally unlimited fluid layer. The solutions were

Downloaded from https://www.cambridge.org/core, on subject to the Cambridge Core terms of use, available at https://www.cambridge.org/core/terms.
https://doi.org/10.1017/CBO9781139034173.006

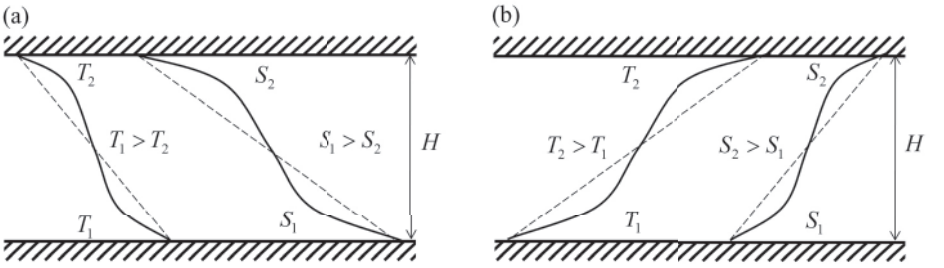

Figure 5.1 Schematic illustration of the bounded diffusive (a) and fingering (b) model. The fluid layer is vertically limited by rigid and slippery horizontal planes with prescribed temperature and salinity values.

sought as a perturbation to the purely conductive state, characterized by uniform vertical temperature and salinity gradients. Despite the similarity of the model formulation to its thermal one-component counterpart (Malkus and Veronis, 1958), the presence of a stabilizing salt gradient did not merely modify the thermal convection problem but resulted in qualitatively different, much richer and, arguably, less intuitive dynamics.

The inclusion of a salt gradient immediately leads to major changes in the linear stability properties of the bounded system. As thermal forcing ($\Delta T = T_1 - T_2$) is increased from zero, the instability initially appears in the form of oscillatory overstable perturbations. Veronis (1965) rationalized this property by offering the following physical argument. In order for direct, monotonically growing, modes to emerge first, they have to be preceded by a marginally stable steady state. Steady infinitesimal motions can occur only when the advection of the mean gradients is balanced by the diffusion of perturbations. The advection–diffusion equations for temperature and salinity (dimensional formulation) reduce to:

$$\begin{cases} w'\bar{T}_z = k_T \nabla^2 T', \\ w'\bar{S}_z = k_S \nabla^2 S'. \end{cases} \tag{5.1}$$

However, diffusion of salt is much slower than the diffusion of heat. Thus, if the background stratification is gravitationally stable ($R_\rho^* = \frac{\beta \bar{S}_z}{\alpha \bar{T}_z} > 1$) or close to neutral ($R_\rho^* \sim 1$) then, in view of (5.1), the density perturbation should be dominated by the haline component $\left(\alpha T' \sim \tau \beta S' \ll \beta S'\right)$. This means that the dynamics of such a system are controlled by the salinity distribution. The governing equations describing the evolution of the salinity field become effectively uncoupled from thermal effects. However, the background salinity stratification is stable and therefore steady infinitesimal convection is impossible; perturbations gradually decay due to molecular dissipation.

Downloaded from https://www.cambridge.org/core, on subject to the Cambridge Core terms of use, available at https://www.cambridge.org/core/terms.
https://doi.org/10.1017/CBO9781139034173.006

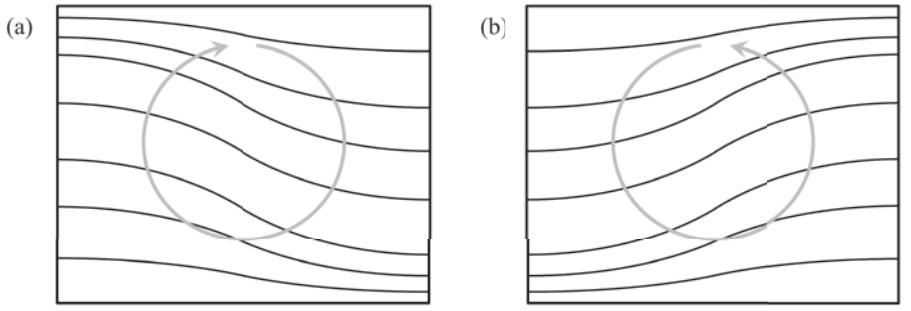

Figure 5.2 Mechanism of the oscillatory diffusive instability in the bounded model. The schematic shows the salinity surfaces for the clockwise (a) and counterclockwise (b) oscillation phases. From Veronis (1965).

This argument suggests that steady circulation in the linear model is permitted only under the rather restrictive conditions of the gravitationally unstable density distribution. Since the existence of a stable steady state is a prerequisite for the direct modes of instability, we arrive at the conclusion that, without oscillatory modes, linear destabilization of the bottom-heavy fluid is impossible. Direct modes are inherently limited in this regard. As will be seen shortly, oscillatory motions are characterized by higher dynamic flexibility – they can tap into the sources of available potential energy that are inaccessible for the direct modes.

The mechanism of overstable oscillations in the bounded bottom-heavy fluid is illustrated in Figure 5.2a,b. The evolutionary pattern of this system is characterized by periodic transitions between the clockwise (a) and counterclockwise (b) circulation patterns. Since heat diffuses much faster than salt, the isotherms tend to be more horizontal than the isohalines. Crowded curves in the upper left-hand region of the regime (a) correspond to saltier and therefore heavier fluid than in the upper right-hand region. Similarly, the fluid in the lower left-hand region is heavier than in the lower right-hand region. The counterclockwise torque produced in this manner reverses the sense of circulation, resulting in the regime indicated in (b). Reproducing the foregoing argument for the system (b), we conclude that the torque is now clockwise, causing the system to reverse the circulation pattern again, recreating the original configuration in (a). The cycle repeats over and over again. Furthermore, when thermal forcing is sufficiently strong, oscillations are not just maintained but systematically increase in amplitude. This scenario provides the physical interpretation for oscillatory diffusive instability in the bounded model. While Veronis' picture, understandably, has some similarities to that of overstable oscillations in the unbounded model (Chapter 1), it is cast in terms of more interesting, and perhaps more relevant for most applications, two-dimensional dynamics.

Downloaded from https://www.cambridge.org/core, on subject to the Cambridge Core terms of use, available at https://www.cambridge.org/core/terms.
https://doi.org/10.1017/CBO9781139034173.006

An analysis of nonlinear effects in the bounded diffusive model brings more surprises. For low diffusivity ratio ($\tau \to 0$), linear theory predicts instability for

$$R > \frac{Pr}{1+Pr} R_S + \frac{27}{4}\pi^4, \tag{5.2}$$

where $R = \frac{g\alpha \Delta T H^3}{\nu k_T}$ is the Rayleigh number based on the thermal component and $R_S = \frac{g\beta \Delta S H^3}{\nu k_T}$ is the salinity Rayleigh number; H is the layer thickness; $\Delta T = T_1 - T_2$ and $\Delta S = S_1 - S_2$ are the temperature and salinity variations across the layer (see Fig. 5.1a). For large Rayleigh numbers, (5.2) is equivalent to the unbounded condition (Chapter 1):

$$R_\rho^* < \frac{Pr+1}{Pr}. \tag{5.3}$$

Thus, while the bounded model permits the instability of bottom-heavy fluids, the instability range is rather narrow for any moderately large Prandtl number. For the heat–salt system ($Pr = 7$) we expect double-diffusive convection for $1 < R_\rho^* < 1.14$.

The linear result (5.3) seems to be at odds with the basic properties of diffusive convection. Laboratory experiments (Chapter 4) as well as field observations, with Arctic staircases being the prime example, offer plenty of evidence for the abundance of double-diffusive structures for density ratios as high as $R_\rho^* \sim 10$. Why then are such phenomena inconsistent with (5.3)? The contradiction is resolved by considering nonlinear effects. Before presenting the supporting analytical and numerical evidence, Veronis (1965) points out that nonlinearity is bound to destabilize the diffusive system. It is natural to expect that an active fully nonlinear circulation acts to homogenize the interior distribution of temperature and salinity. The "interior" in this context refers to a region separated from the upper and lower boundaries where temperature and salinity values are prescribed. The tendency of the circulation to mix the interior is opposed by molecular diffusion, acting to restore the stratification. This balance applies for both temperature and salinity, but diffusivity of salt is extremely low and therefore the tendency to restore interior salinity stratification is very weak. Thus, the interior salinity would be homogenized more than temperature. In this case, the interior density distribution is controlled by the (negative) temperature gradient, resulting in top-heavy stratification. The interior density distribution becomes gravitationally unstable, supporting vigorous overturning circulation. This argument – in contrast to the linear analysis – predicts that the motion in the bounded model can be maintained even if the variation in the thermal component of density is a small fraction of the corresponding salinity variation ($\alpha\,|\Delta T| \ll \beta\,|\Delta S|$).

Veronis unambiguously confirmed his physical argument through fully nonlinear simulations and an analytical model based on the highly truncated Fourier

Downloaded from https://www.cambridge.org/core, on subject to the Cambridge Core terms of use, available at https://www.cambridge.org/core/terms.
https://doi.org/10.1017/CBO9781139034173.006

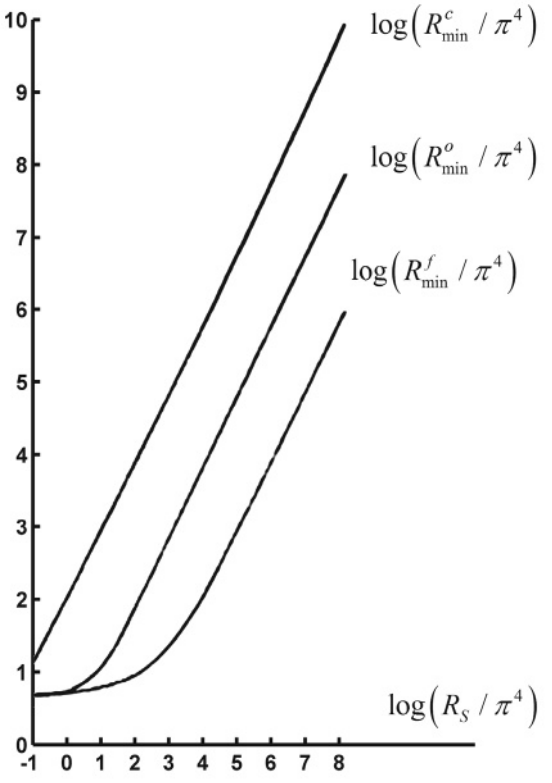

Figure 5.3 The values of three critical thermal Rayleigh numbers $R^c_{\min}$,$R^o_{\min}$ and $R^f_{\min}$ (see the text) are plotted as a function of the haline Rayleigh number R_S. From Veronis (1965).

representation of all variables. Figure 5.3 shows the values of three critical thermal Rayleigh numbers required for (i) the destabilization of the infinitesimal direct mode ($R^c_{\min}$), (ii) the infinitesimal oscillatory instability ($R^o_{\min}$) and (iii) the maintenance of finite amplitude motion ($R^f_{\min}$). All minimal thermal Rayleigh numbers are plotted as a function of the haline Rayleigh number (R_S). The Rayleigh number for linear direct instability is two orders of magnitude higher than for oscillatory modes and, perhaps an even more striking result, exceeds $R^f_{\min}$ by four orders of magnitude.

Numerical integrations reveal another counterintuitive feature of the bounded diffusive system. Although the preferred mode of linear evolution is oscillatory, the system ultimately evolves in time to a regular steady state. This fundamentally nonlinear steady state could be approached either through growth of the oscillatory modes (for $R > R^o_{\min}$) or, alternatively, by introducing a sufficiently large initial

Downloaded from https://www.cambridge.org/core, on subject to the Cambridge Core terms of use, available at https://www.cambridge.org/core/terms.
https://doi.org/10.1017/CBO9781139034173.006

perturbation, which makes the transition to a finite amplitude steady state possible even for $R < R^o_{\min}$. The formation of the steady state for $R < R^o_{\min}$ is interesting since the *infinitesimal* steady states are possible only for much larger thermal Rayleigh numbers ($R^c_{\min} \gg R^o_{\min}$). In this regard, bounded diffusive convection is rather unusual. In the majority of instability studies (e.g., one-component convection) linear theory offers valuable insights, qualitatively applicable to the finite amplitude evolution of the system. For diffusive convection, all bets are off. The diffusive problem is principally nonlinear.

Numerical simulations in Veronis (1968) revealed that the more realistic representation of fluid (relative to the minimal model in Veronis, 1965) has a generally stabilizing effect on the system. Specific calculations were restricted to the top-heavy configuration, which takes the analysis somewhat beyond the scope of this monograph – double-diffusion in gravitationally stable configurations. However, several lessons learned from Veronis' analysis have a generic character and are likely to apply to bottom-heavy double-diffusive systems. One conclusion concerns the counter-gradient density flux. The solute gradient in the immediate vicinity of the boundary is necessarily sharper than the temperature gradient, and therefore the net tendency would be to maintain gravitationally stable boundary layers. In the interior regions, characterized by convective overturns, density flux is necessarily downward. Thus, in the boundary layers, density flux is counter-gradient and the effective diffusivity of density is negative. Quantifying this idea, Veronis (1968) goes on to predict a specific value of the boundary layer diffusivity for the nearly neutral background stratification ($R \approx R_S$):

$$k_\rho \sim -(k_T k_S)^{\frac{1}{2}}. \tag{5.4}$$

Another suggestive observation involves a systematic increase in the period of oscillations in time for the growing oscillatory modes. For a relatively narrow range of intermediate thermal Rayleigh numbers (R), the ultimate state of the system is represented by the finite amplitude oscillations, with the amplitude increasing with R. However, for sufficiently large values of R, finite amplitude oscillatory instability ultimately settles into a steady convective pattern. The tendency for the oscillation period to increase with increasing perturbation amplitude may prove to be the key for explaining the transition from linear oscillatory growth to eventual steady circulation observed in most simulations of diffusive systems.

Finally, Veronis suggests that the heat flux of the fully equilibrated diffusive system should be comparable to the corresponding heat flux observed in thermal convections for the same Rayleigh numbers. The rationale is rather straightforward. Strong finite amplitude convection would homogenize salinity in the interior zone and, since the diffusivity of salt is very low, the tendency to restore the stratification

Downloaded from https://www.cambridge.org/core, on subject to the Cambridge Core terms of use, available at https://www.cambridge.org/core/terms.
https://doi.org/10.1017/CBO9781139034173.006

by means of molecular diffusion is weak. In this case, the inhibiting effect of the solute gradient will be reduced, and the fluid can convect nearly as much heat as it does in the absence of the solute. The available simulations for the bounded diffusive system confirm this conjecture. However, the reader is reminded that the laboratory experiments with diffusive interfaces, discussed in Chapter 4, can yield heat transports an order of magnitude larger than in corresponding thermal convection experiments. This underscores differences between the bounded and two-layer models. In both cases, heat transport is constrained by the diffusion of temperature through thin and strongly stratified boundary layers. However, in the bounded model the vertical velocity vanishes identically at the boundary and therefore molecular diffusion there is the only means for heat transfer. In the case of the two-layer configuration, however, this constraint is not nearly as severe – the interface is deformable and therefore the possibility exists for the eddy-induced transport of heat and salt.

Since Veronis' studies, the bounded diffusive model has been investigated in much greater detail a number of times. Huppert and Moore (1976) performed a comprehensive numerical analysis of the Veronis problem. Steady finite amplitude solutions were obtained and examined for linearly stable bottom-heavy stratification. Systematic exploration of the (R, R_S) parameter space made it possible to classify all nonlinear solutions into four major categories. As the thermal Rayleigh number increases, the thermohaline system undergoes transitions from (i) simple quasi-harmonic oscillations to (ii) more complicated periodic oscillations, then to (iii) aperiodic and, finally, to (iv) time-independent solutions. Somewhat counterintuitively, an increase in the Rayleigh number in the diffusive model suppresses the disordered motion. For certain parameters, two different solutions exist. Numerous instances of hysteresis were found in simulations in which an increase in Rayleigh number was followed by its decrease.

The key numerical results in Huppert and Moore (1976), particularly with regard to the dynamics of steady solutions, were rationalized by a complementary analytical study (Proctor, 1981). The rich dynamics of diffusive systems motivated numerous follow-up studies aimed to describe bifurcations and chaotic behavior observed in numerical simulations (Moore and Weiss, 1990; Knobloch *et al*., 1992; among others). In terms of explaining diffusive dynamics from first principles, particularly promising are attempts to formulate Fourier-truncated models, which reduce the governing differential equations to a small set of ordinary differential equations (e.g., Da Costa *et al*., 1981). These relatively simple low-order models have proven to be successful in capturing the behavior of the full system and in revealing the zero-order dynamics at play. Other applications of the bounded diffusive model include the analysis of the effects associated with non-uniformities of the background stratification (Balmforth *et al*., 1998; Walton, 1982) and the

Downloaded from https://www.cambridge.org/core, on subject to the Cambridge Core terms of use, available at https://www.cambridge.org/core/terms.
https://doi.org/10.1017/CBO9781139034173.006

appearance of spatially localized nonlinear states (Batiste *et al*., 2006; Bergeon and Knobloch, 2008a,b).

An interesting approach to the analytical modeling of double-diffusive convection involves the prediction of the upper bound on the flux of the unstably stratified component using variational principles. The basic idea of this method has been introduced in pioneering studies by Malkus (1954) and Howard (1963) for thermal convection. In view of the complexities of the governing equations in fluid mechanics, the upper bound theory does not attempt to search for actual solutions but, instead, places bounds on some of their average properties. The method is based on the integral relations (power integrals) derived from, but much simpler than, the original system. Using a series of algebraic inequalities, it is usually possible to rigorously deduce upper limits for the vertical transport of the diffusing properties. The upper bound theory has been widely and successfully applied to various fluid dynamical problems (Joseph, 1976; Doering and Constantin, 1996; Kerswell, 1998). While double-diffusive convection appears to be well suited for the application of the upper bound theory, only a few such attempts (Stern, 1982; Balmforth *et al*., 2006) have been reported.

The double-diffusive version of the upper bound theory is more challenging and intriguing than the convective case, particularly since it exhibits a remarkably rich array of dynamics. It uses the same power integrals for T and S that emerge in one-component convection but also adds a crucial mixed integral constraint, representing the interplay of temperature and salinity perturbations. Stern (1982) applied the upper bound theory to the diffusive case, whereas Balmforth *et al*. (2006) examined both diffusive and fingering regimes. The ultimate goal of any bounding exercise is to formulate the upper bound that is sufficiently close to the physically realized fluxes. Although double-diffusive theories may not yet have reached this goal, the physical insights brought about by such bounding models are already evident. Conversely, the problem of double-diffusive convection between two rigid horizontal planes offers an attractive testing ground for the development of new methods for the upper bound theory. This line of research is promising and should be pursued much further.

Before moving on to the next topic, we should note some difficulties regarding the application of the bounded diffusive model to observed phenomena. To the best of the author's knowledge, no double-diffusive configuration in nature involves setting specific temperature and salinity values at the vertical boundaries. Problems arise even in the controlled setting of laboratory experiments. Perhaps closest to the bounded model comes a setup used by Krishnamurti (2003, 2009), who maintained the vertical finger-favorable T–S differences by flushing the reservoirs located at the top and bottom of the experimental tank (Chapter 4). This laboratory configuration has not yet been used in the diffusive regime.

Downloaded from https://www.cambridge.org/core, on subject to the Cambridge Core terms of use, available at https://www.cambridge.org/core/terms.
https://doi.org/10.1017/CBO9781139034173.006

Nevertheless, the bounded model is likely to be relevant, albeit in an abstract and qualitative sense, to laboratory and oceanic examples of diffusive convection. A generic pattern realized in this model consists of thin boundary layers near the solid horizontal planes, controlled by the molecular dissipation of heat and salt, and a gravitationally unstable interior. The dynamics of diffusive layers in nature are similar. The key feature is the interplay between molecular diffusion acting across thin interfaces and convection in the adjacent mixed layers. Therefore, it is our belief that insights generated by studies of the bounded diffusive model (Veronis, 1965, 1968; Knobloch *et al*., 1992; Balmforth and Biello, 1998; Balmforth *et al*., 1998) have general applicability. The analogy between the bounded *salt-finger* model – our next topic – and realizations in nature is more tenuous, although certain dynamic similarities do exist.

5.2 Salt-finger layer

Consider the salt-finger configuration in Figure 5.1b. As previously, the bounded model prescribes temperature and salinity values at the rigid slippery vertical boundaries, although in this case both temperature and salinity increase upward ($T_2 > T_1$, $S_2 > S_1$). The aspects of fingering adequately addressed by the bounded model include the pattern selection problem and analysis of the finger-induced transport.

Planform selection

One of the first bounded finger models was developed by Straus (1972), who numerically obtained two-dimensional finite amplitude steady solutions and examined their stability with respect to three-dimensional perturbations. Computational constraints at that time prevented the author from approaching the parameter regimes that would be relevant for most applications. Nevertheless, this study raised some intriguing questions. For instance, stability analysis of the finite amplitude two-dimensional (roll-type) solutions suggested that they are stable with respect to three-dimensional perturbations as long as the horizontal wavelength is comparable to the height of the fluid layer. The stability of salt-finger rolls suggests that such two-dimensional structures should be realized in nature. The latter proposition is at odds with laboratory observations (Shirtcliffe and Turner, 1970), which clearly revealed the preference for three-dimensional patterns best described as squares (Fig. 4.5).

An attempt to identify the cause of the disagreement was made by Proctor and Holyer (1986), who treated the problem using an asymptotic expansion pivoted about the marginally unstable point. The problem of pattern selection in the

Downloaded from https://www.cambridge.org/core, on subject to the Cambridge Core terms of use, available at https://www.cambridge.org/core/terms.
https://doi.org/10.1017/CBO9781139034173.006

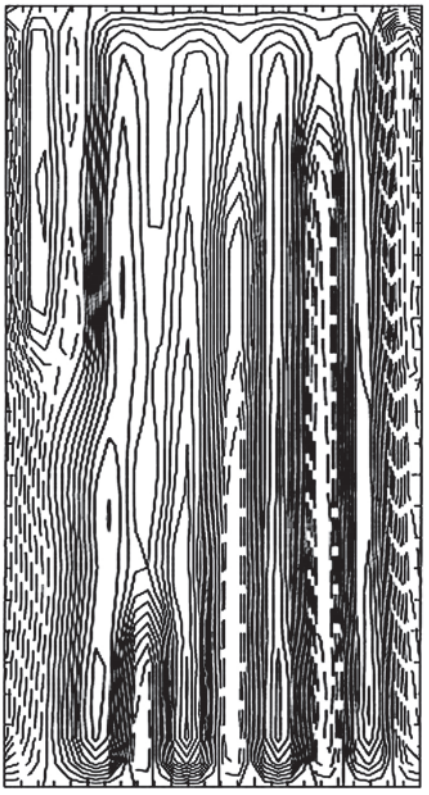

Figure 5.4 Vertical cross-section of the fully developed temperature perturbation (T') in the bounded numerical simulation (salt-finger case). The computational domain corresponds to $5 \times 5 \times 10$ fastest growing finger wavelengths. From Radko and Stern (2000).

salt-finger regime is challenging because linear instability theory (Chapter 2) provides no guidance with respect to the preferred planform. Identical growth rates can be achieved by a variety of horizontal structures and, from the perspective of linear theory, two-dimensional rolls are as likely to be realized as square cells. Apparently, the key to the planform selection lies in fundamentally nonlinear interactions between different modes present in the equilibrated state. Therefore, Proctor and Holyer (1986) incorporated the leading-order nonlinear effects by expanding in the small parameter $\frac{L}{H} \ll 1$ representing the ratio of the typical width of fingers (L) to the layer height (H). Their model assumed that fingers are vertically elongated throughout the fluid layer, thereby excluding from consideration structures of limited – comparable to the salt-finger width – vertical extent (Fig. 5.4). The weakly nonlinear analysis led the authors to conclude, in conflict with observations, that the roll-type planforms are preferred over the square cells.

Downloaded from https://www.cambridge.org/core, on subject to the Cambridge Core terms of use, available at https://www.cambridge.org/core/terms.
https://doi.org/10.1017/CBO9781139034173.006

The suggestion of the dynamic preference for square fingers was supported by the laboratory experiments referenced in Schmitt (1994a). In these experiments, salt fingers were generated in a triangular tank. The geometry of the container did not affect the planform: fingers remained rectangular. It should be noted that the planform selection has been discussed mostly in connection with laboratory experiments: fingers in the ocean are less accessible and more irregular. However, an interesting example was reported by Osborn (1991), who observed asymmetric salt fingers in the near-surface zone of the ocean. These fingers were characterized by narrow downward plumes separated by a weaker and broader upwelling. The spacing between adjacent fingers was consistent with the prediction of the fastest growing finger model. Schmitt demonstrated that such asymmetric structures can be obtained by superposing several fastest growing modes with differing horizontal wavenumber components. Although the selection mechanism of asymmetric structures has never been fully explained, it was hypothesized (Osborn, 1991; Schmitt, 1994a) that surface evaporation effects could have played some role.

The next attempt to solve the planform selection puzzle was made by Radko and Stern (2000). As in Proctor and Holyer (1986), this study was based on a weakly nonlinear asymptotic expansion. However, the small parameter $((R_\rho\tau)^{-1} - 1)$ in Radko and Stern measured the separation of parameters from the marginally stable point for salt fingering ($R_\rho = \tau^{-1}$). No assumption was made regarding the relative difference in vertical and horizontal scales, which made it possible to adequately represent thin boundary layers at the edges of the finger zone. These boundary layers, clearly visible in Figure 5.4, proved to be essential in the pattern selection process. Figure 5.5 shows a numerical experiment initiated by slightly perturbed rolls. The horizontal temperature pattern slowly transforms from a quasi two-dimensional structure to remarkably regular square cells. Particularly suggestive is the sequence of events – the transition from rolls to cells starts within the boundary layers and then spreads throughout the elongated fingers in the interior. The significance of boundary layers for the planform selection was confirmed by asymptotic analysis. Radko and Stern (2000) demonstrated that (i) two-dimensional rolls are unstable with respect to cross-roll perturbations and (ii) an approximation which assumes that the vertical scale of the boundary layer exceeds the salt-finger width immediately leads to the opposite (and erroneous) conclusion. The observed preference for square cells was attributed to the instability of solutions with non-square planforms, which resolved the conundrum posed by Proctor and Holyer (1986).

Vertical transport

In addition to the dynamics of the horizontal pattern selection, the bounded salt-finger model has brought some insight into the mechanisms controlling the

Downloaded from https://www.cambridge.org/core, on subject to the Cambridge Core terms of use, available at https://www.cambridge.org/core/terms.
https://doi.org/10.1017/CBO9781139034173.006

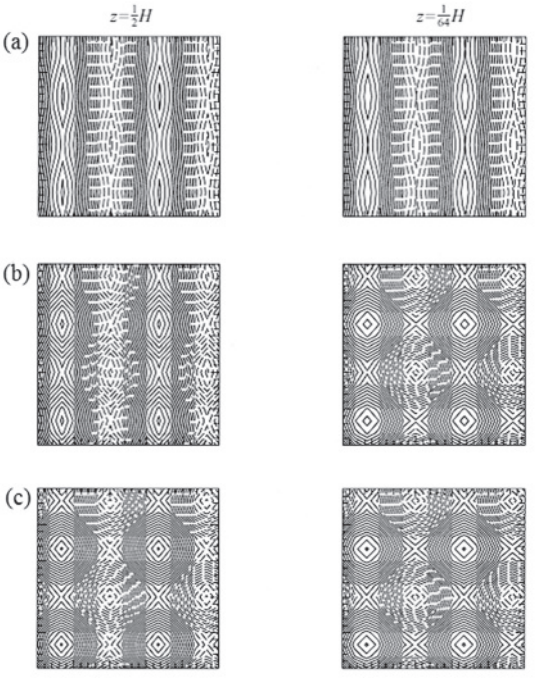

Figure 5.5 Transition from rolls to square cells in a numerical simulation. Shown are the horizontal cross-sections of temperature across the boundary layer (right) and across the interior region (left) at various stages. The time increases from (a) to (c). Transition to the square-cell planform starts with the boundary layer (b) but eventually is completed at all levels (c). From Radko and Stern (2000).

vertical T–S transport across the salt-finger layer. For two-layer systems (Chapter 4) dimensional arguments lead to Turner's (1967) flux law (4.6). These dimensional arguments do not necessarily apply to the bounded configuration (Fig. 5.1) since the bounded model involves an additional *independent* dimensional parameter – thickness of the salt-finger layer (H). Nevertheless, numerical simulations in Radko and Stern (2000) revealed that the bounded model is well described by the four-thirds flux law. A series of calculations in which density ratio and molecular parameters were fixed, but the height of the finger layer varied by an order of magnitude, produced a nearly uniform flux law coefficient $C'_S = \frac{\alpha F_S}{(\alpha \Delta S)^{\frac{4}{3}}}$. In an attempt to rationalize this unexpected behavior, Radko and Stern (2000) developed an analytical model for the vertical transport, predicting

$$C'_S \propto H^{-\frac{1}{10}} (\Delta S)^{-\frac{1}{30}} . \tag{5.5}$$

The exponents $-1/10$ and $-1/30$ in (5.5) correspond to extremely weak dependences on layer height and overall T–S variation and therefore the flux law

Downloaded from https://www.cambridge.org/core, on subject to the Cambridge Core terms of use, available at https://www.cambridge.org/core/terms.
https://doi.org/10.1017/CBO9781139034173.006

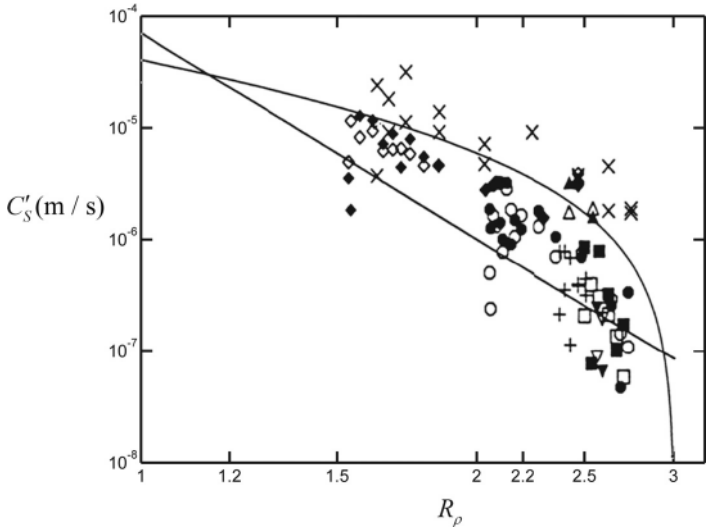

Figure 5.6 Flux law constant C'_S as a function of density ratio in the bounded model of Radko and Stern (2000) indicated by the solid curve and in the laboratory experiments of Taylor and Veronis (1996) marked by various signs. The straight line is an average of the laboratory experiments of Griffiths and Ruddick (1980). From Radko and Stern (2000).

coefficient is effectively determined by the density ratio, as in Turner's four-thirds flux law.

A perhaps even more surprising and suggestive finding of Radko and Stern (2000) is that the fluxes obtained for the bounded model were consistent with the fluxes in the laboratory two-layer experiments (Chapter 4) in which the finger zone is sandwiched between two well-mixed reservoirs. Figure 5.6 presents a plot of the flux law coefficient (5.5) from a bounded layer model (Radko and Stern, 2000) superimposed on a series of two-layer experiments (Taylor and Veronis, 1996). Both the magnitude of C'_S in experiments and its variation with the density ratio is captured by the bounded model. What makes this result particularly intriguing is that the model does not contain any significant adjustable parameters and therefore the comparison is objective. The agreement between the laboratory- and model-based estimates of C'_S in Figure 5.6 suggests that the dynamics of the finger zone in the bounded model and in two-layer experiments are similar. It is plausible that the vertical velocity of individual fingers in experiments is greatly reduced as they approach large-scale plumes in the convectively mixing layers. If so, the matching conditions at the boundary between the salt-finger zone and the mixed layers can be approximated by simple rigid lid conditions, and the bounded model can be used to explain the dynamics of two-layer experiments.

Downloaded from https://www.cambridge.org/core, on subject to the Cambridge Core terms of use, available at https://www.cambridge.org/core/terms.
https://doi.org/10.1017/CBO9781139034173.006

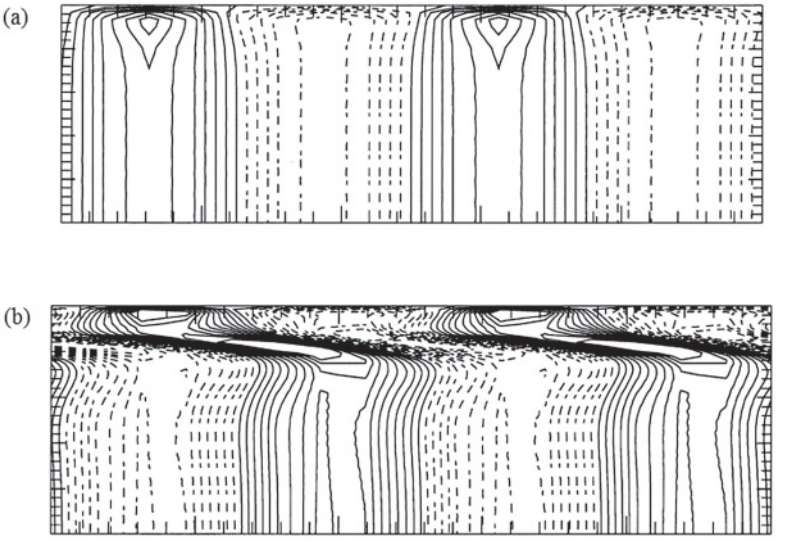

Figure 5.7 The temperature patterns in the boundary layer in two calculations with different values of H. The boundary layer Rayleigh number in (a) is $Ra = 1440$ and in (b) is $Ra = 2800$. The boundary layer for the low Ra regime is stable and laminar, while in the high Ra case it is distorted by the local instability. From Radko and Stern (2000).

Height of the finger zone

An obvious difference between the bounded model and typical two-layer laboratory experiments is related to the selection of the thickness of the finger layer (H). In the bounded model, the layer thickness is a free parameter, but in two-layer experiments it is controlled by the variations in temperature and salinity across the mixed layers (ΔT, ΔS). Still, the bounded model brings some insight into the mechanisms that could be involved in the selection of H. Radko and Stern (2000) examined a series of bounded model simulations in which H was systematically increased, and noticed that at a certain point ($H = H^*$) the flow field undergoes a dramatic transition. For relatively low values of H, temperature and salinity patterns are regular and steady. However, when H exceeds a critical value (H^*), the flow becomes disorganized and time-dependent, which is suggestive of the onset of a secondary instability. This instability has a local character and it is limited to thin conductive boundary layers forming near the vertical boundaries (Fig. 5.7).

The origin of the secondary boundary layer instabilities is clear. As the vertical velocity near the rigid boundaries is suppressed, the vertical *advective* fluxes in the boundary layers ($\alpha\overline{w'T'}$, $\beta\overline{w'S'}$) are greatly reduced relative to that in the interior, which is compensated by the increase in *conductive* transport ($k_T\alpha\bar{T}_z$, $k_S\beta\bar{S}_z$).

Downloaded from https://www.cambridge.org/core, on subject to the Cambridge Core terms of use, available at https://www.cambridge.org/core/terms.
https://doi.org/10.1017/CBO9781139034173.006

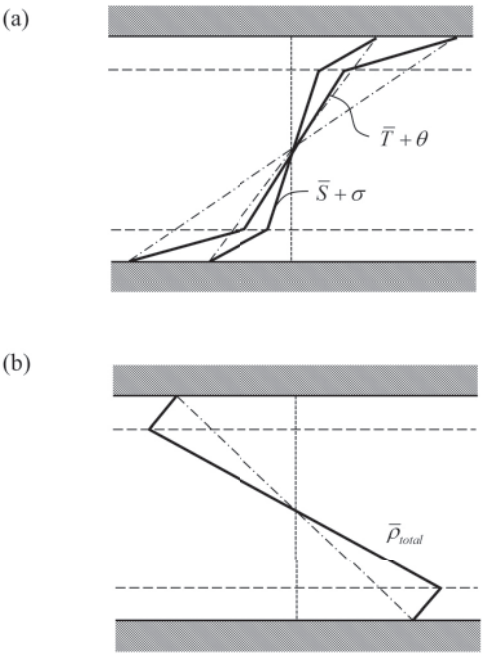

Figure 5.8 Schematic diagram of the horizontally averaged profiles of temperature and salinity (a) and density (b) in the bounded steady state. From Radko and Stern (2000).

Since vertical density fluxes due to heat and salt transport by fingers are comparable ($\gamma \sim 1$), we expect that in the boundary layers $k_T \alpha \bar{T}_z \sim k_S \beta \bar{S}_z$ and therefore $\alpha \bar{T}_z \ll \beta \bar{S}_z$. The latter inequality implies that the density stratification in the boundary layers is gravitationally unstable ($\bar{\rho}_z > 0$) in contrast to the stable interior ($\bar{\rho}_z < 0$), as shown in the schematic in Figure 5.8. A well-known criterion for the instability of the gravitationally unstable layers is based on the thermohaline Rayleigh number (*Ra*). When *Ra* exceeds a critical value on the order of a thousand, vigorous instabilities are expected to occur, which is readily confirmed by inspection of the boundary layers in Figure 5.7.

Calculations in Radko and Stern (2000) were performed for $\tau = 1/3$ – a model of the sugar–salt experiment. The order-one value of the diffusivity ratio implies comparable scales for the haline and thermal boundary layers and thereby simplifies analytical development. The local thermohaline Rayleigh number is given by

$$Ra = \frac{gh^4}{\nu}\left(\frac{\bar{S}_z}{k_S} - \frac{\bar{T}_z}{k_T}\right), \tag{5.6}$$

where h is the thickness of boundary layers. The boundary layer Rayleigh number was evaluated for the calculation in Figure 5.7a (regular boundary layer), resulting in $Ra = 1440$, and for the visibly unstable boundary layer in Figure 5.7b, yielding

Downloaded from https://www.cambridge.org/core, on subject to the Cambridge Core terms of use, available at https://www.cambridge.org/core/terms.
https://doi.org/10.1017/CBO9781139034173.006

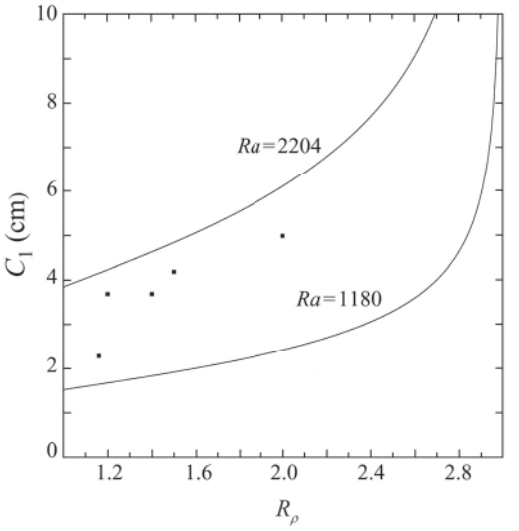

Figure 5.9 Comparison of the theoretical prediction of the coefficient C_1 in the interfacial thickness law (4.8) with the results of the laboratory experiments (Linden 1978). The analytical theory suggests that the $C_1(R_\rho)$ functions are controlled by the values of the boundary layer Rayleigh number Ra and the slope of the corresponding theoretical curves is in apparent agreement with the experimental data. From Radko and Stern (2000).

$Ra = 2800$. Analytical theory suggests that the local boundary layer Rayleigh number is controlled by the overall height of the finger layer ($Ra \propto H^{0.4}$), which explains destabilization of the boundary layers at sufficiently high H. The critical thickness (H^*) corresponding to the onset of the boundary layer instability can be estimated by requiring $Ra \sim 1000$.

Limited evidence from numerical and laboratory two-layer experiments (Chapter 4) suggests that the dynamics of such systems also undergo boundary layer instabilities and are profoundly affected by them. Numerical simulations in Shen (1989) revealed the appearance of local density inversions at the edges of the finger zone. Shen hypothesized that these inversions are essential for the breakup of fingers. Such transitional zones between convecting layers and finger interfaces are also visible in the shadowgraphs of laboratory experiments (Linden, 1978). Therefore, it is sensible to assume that the local instability of the top-heavy transitional zones is involved in the arrest of the spatial spreading of the finger zone in two-layer experiments. Radko and Stern (2000) hypothesized that the equilibrium thickness of the finger layer in two-layer experiments corresponds to the marginally unstable transitional zone ($Ra \sim 1000$). This theory finds some support in laboratory data. Figure 5.9 presents the coefficient of the thickness law (4.8) $C_1 = H(\beta\Delta S)^{\frac{1}{3}}$ deduced from measurements in Linden (1978) and predicted by

Downloaded from https://www.cambridge.org/core, on subject to the Cambridge Core terms of use, available at https://www.cambridge.org/core/terms.
https://doi.org/10.1017/CBO9781139034173.006

the bounded model for selected values of Ra. All experimental points belong to the area corresponding to the boundary layer Rayleigh numbers in the range of $Ra \sim 1000$–2000. Such consistency lends credence to the idea of thickness control by the secondary instabilities of the top-heavy boundary layers forming near the boundaries of the salt-finger interface.

Before concluding the discussion of the bounded model, a few words of caution are in order. Based on the existing evidence, we can claim with some confidence that the bounded model is relevant for the two-layer laboratory experiments, particularly for the sugar–salt case. The boundary layers at the extremities of the finger zone in these experiments (Fig. 4.4) are well defined and appear to be dynamically similar to those in the bounded model. However, the bounded dynamics – interesting as they may be in their own right – are not applicable to all instances of fingering. The relevance of the bounded finger model has to be reexamined on a case-by-case basis. In most cases, including typical oceanographic configurations, salt fingers may be better described by the unbounded model presented in Chapter 3.

Downloaded from https://www.cambridge.org/core, on subject to the Cambridge Core terms of use, available at https://www.cambridge.org/core/terms.
https://doi.org/10.1017/CBO9781139034173.006